JOURNAL OF GEOPHYSICAL RESEARCH, VOL. 113, A05308, doi:10.1029/2007JA012542, 2008

Global distribution and interannual variations of mesospheric and lower thermospheric neutral wind diurnal tide: 1. Migrating tide

Q. Wu,[1,2] D. A. Ortland,[3] T. L. Killeen,[1] R. G. Roble,[1] M. E. Hagan,[1] H.-L. Liu,[1] S. C. Solomon,[1] Jiyao Xu,[2] W. R. Skinner,[4] and R. J. Niciejewski[4]

Received 14 May 2007; revised 6 January 2008; accepted 24 January 2008; published 17 May 2008.

[1] Using the TIMED Doppler interferometer (TIDI) mesospheric and lower thermospheric neutral-wind multiyear data set (2002–2007) and NCAR TIME General Circulation Models (GCM) 1.2 annual run results (2002–2005) at the TIDI sampling points, we study the migrating diurnal tide's global distribution, interannual, and seasonal variations in connection with the mean zonal wind interannual variations. A strong quasi-biennial oscillation (QBO) effect on the diurnal tide was observed in the TIDI data and reproduced to a lesser degree in the TIME-GCM run. The migrating diurnal tide amplitude is larger during the eastward phase of the stratospheric QBO and weaker during the westward phase. Westward mesospheric equatorial mean zonal winds appeared during the eastward phase of the stratospheric QBO (in 2002, 2004, and 2006). The strongest QBO effect on both the migrating diurnal tide and mean zonal winds was observed during the March equinox. The stronger tides may be related to the weaker gravity wave filtering in the stratosphere during the eastward phase stratospheric QBO. The TIDI data also exhibit large interhemispheric asymmetry. The westward mean zonal winds in the mesosphere appeared to be associated with the enhanced diurnal tide. The TIME-GCM 1.2 diurnal tide amplitudes are in general smaller than those observed by the TIDI instrument. Limited vertical spatial resolution for the TIME-CGM 1.2 is suggested as the cause. Future improvements are expected with a higher spatial resolution in the model.

Citation: Wu, Q., D. A. Ortland, T. L. Killeen, R. G. Roble, M. E. Hagan, H.-L. Liu, S. C. Solomon, J. Xu, W. R. Skinner, and R. J. Niciejewski (2008), Global distribution and interannual variations of mesospheric and lower thermospheric neutral wind diurnal tide: 1. Migrating tide, *J. Geophys. Res.*, *113*, A05308, doi:10.1029/2007JA012542.

1. Introduction

[2] The diurnal tide is the most prominent dynamics feature of the mesosphere and lower thermospheric (MLT) region. The MLT diurnal tide has both significant migrating and nonmigrating components. The migrating tide is synchronous with the Sun an effect caused by solar UV radiation absorption by stratospheric ozone and tropospheric water vapor. Studies of the MLT migrating tides have a long history [e.g., *Chapman and Lindzen*, 1970; *Forbes*, 1982a, 1982b; *Vial*, 1989]. Owing to strong forcing, the migrating diurnal tide is much stronger than the nonmigrating tide in most cases.

[3] Both ground-based and satellite observations have revealed many important features of the diurnal tide. Ground-based observations have established seasonal and interannual variations of the MLT diurnal tide at various latitudes [e.g., *Manson et al.*, 1988, 1989, 1999; *Vincent et al.*, 1998; *She et al.*, 2004; *Yuan et al.*, 2006]. By combining observations from various locations, *Pancheva et al.* [2002] were able to assemble a global picture of the diurnal tide, but some large gaps in coverage remain.

[4] Satellite observations from the HRDI and WINDII instruments on board the UARS satellite and the TIDI from the TIMED satellite have provided a global view of the diurnal tide [*Burrage et al.*, 1995; *Wu et al.*, 1995; *Hays et al.*, 1994; *Morton et al.*, 1993; *McLandress et al.*, 1994, 1996; *Lieberman and Hays*, 1994; *Khattatov et al.*, 1997a; 1997b; *Yudin et al.*, 1998; *Wu et al.*, 2006; *Killeen et al.*, 2006]. More significantly, satellite observations also enabled researchers to separate nonmigrating tides from migrating tides [e.g., *Forbes et al.*, 2003a, 2003b; *Oberheide et al.*, 2005, 2006].

[5] The migrating diurnal tide has a strong seasonal variation. The tide reaches large amplitudes during the March and September equinoxes and has smaller values during the June and December solstices. Both ground and satellite observations show this consistent behavior. Various tide models, such as the Global Scale Wave Model (GSWM), also show the same seasonal changes in tidal

[1]High Altitude Observatory, National Center for Atmospheric Research, Boulder, Colorado, USA.
[2]Key Laboratory for Space Weather, Center for Space Science and Applied Research, Chinese Academy of Sciences, Beijing, China.
[3]Northwest Research Associates, Bellevue, Washington, USA.
[4]Space Physics Research Laboratory, University of Michigan, Ann Arbor, Michigan, USA.

0148-0227/08/2007JA012542$09.00

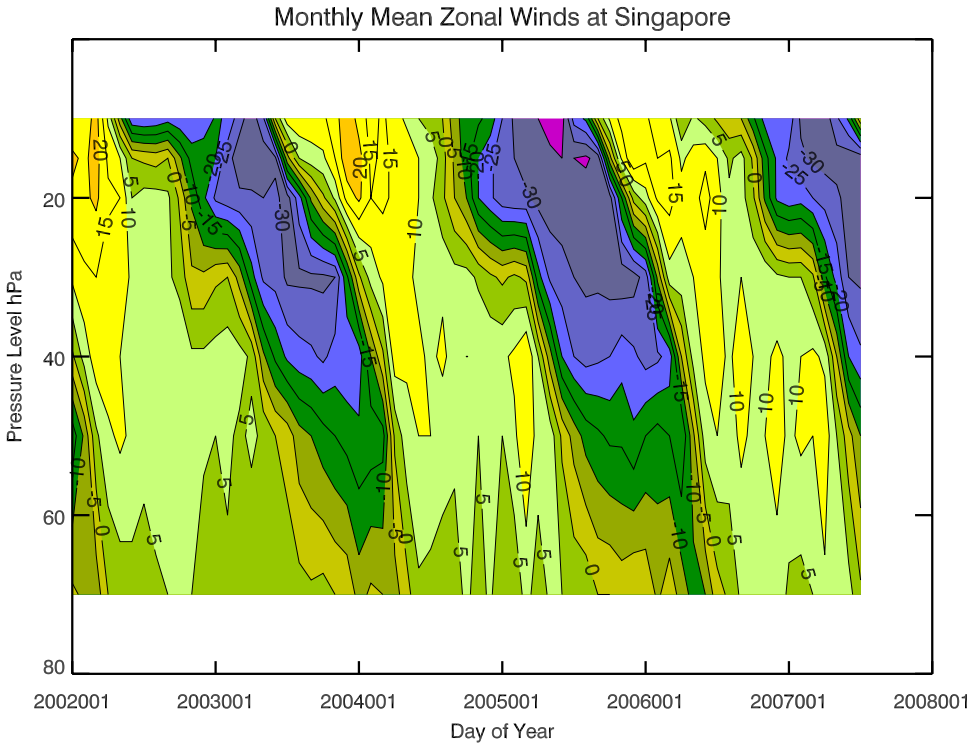

Figure 1. Monthly stratospheric zonal winds over Singapore. Monthly averaged radiosonde stratospheric winds over Singapore from 2002 to 2007. The contour step is 5 m/s.

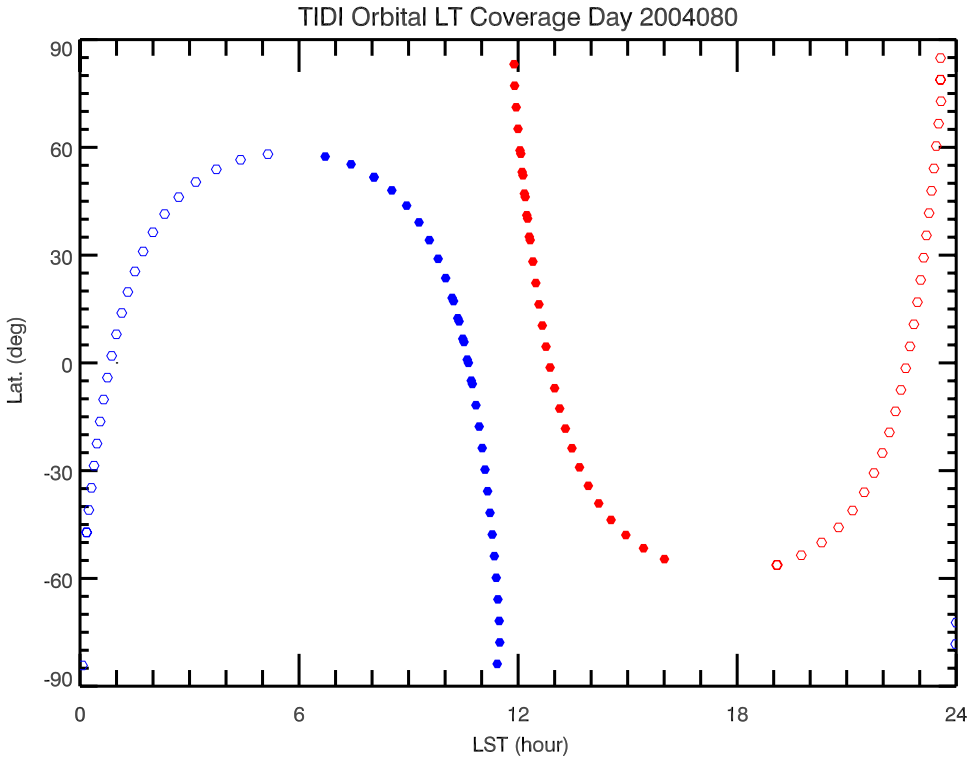

Figure 2. TIDI sampling points in local time. The blue track (southern) is for the cold side of TIMED satellite (away from the Sun) whereas the red track (northern) is for the warm side (toward the Sun). The solid dots are for daytime and hollow dots are for nighttime. The ascending (nighttime) and descending (daytime) nodes are plotted.

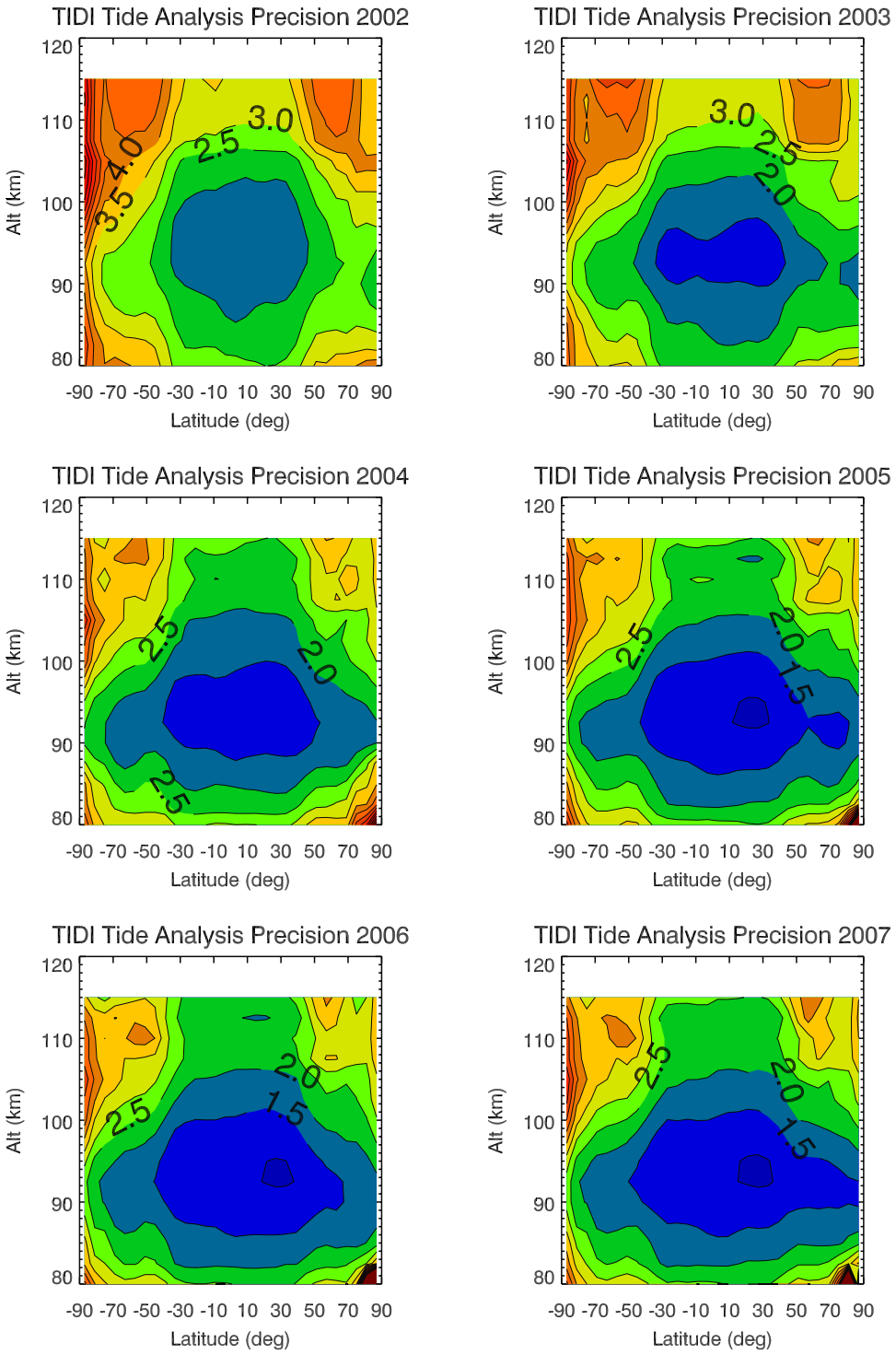

Figure 3. TIDI tide analysis precision. The horizontal grid size is 6 degree and vertical is 2.5 km. Each sampling will have about 900 raw data point from a 60 d slighting window. Precisions are estimated for the 6 years during the March equinox. The gradual improvement of the precision from 2002 to 2005 is due to reduction of the ice on the TIDI optics. The contour step is 0.5 m/s.

amplitude [*Hagan et al.*, 1999a; *Hagan and Forbes*, 2002, 2003].

[6] Moreover, the diurnal tide also exhibits a strong interannual variation closely related to the stratospheric quasi-biennial oscillation (QBO) [*Burrage et al.*, 1995; *Hagan et al.*, 1999b, *Lieberman*, 1997; *Vincent et al.*, 1998]. Recently, using TIMED SABER temperature data, *Huang et al.* [2006] have examined the QBO effects on the mesospheric temperature diurnal tide. It has long been suggested that the diurnal tide QBO effect is related to the mesospheric mean zonal wind QBO-like variations caused by the direct link via the advection terms in the tidal equation [*Mayr and Mengel*, 2005]. Observations have shown that the migrating diurnal tide increases (decreases)

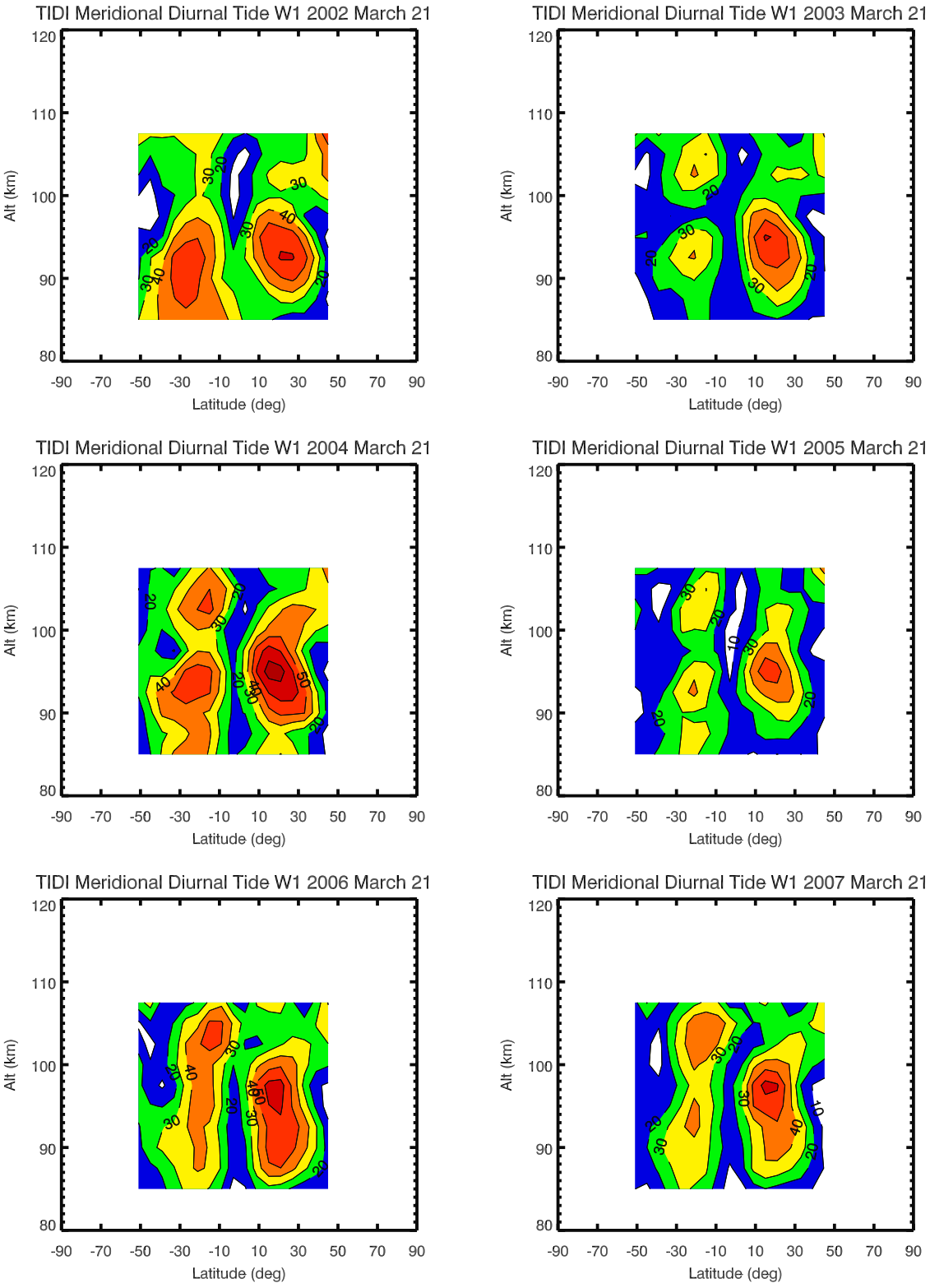

Figure 4a. TIDI migrating diurnal tide westward one (W1) in meridional winds during the March equinox. The migrating diurnal tide amplitude altitude and latitude variations based on 60-d period observations the first of which centered at day 81 (March 21). For easier comparison, the data from the same season of the six different years are plotted on the same page. The contour step is 10 m/s.

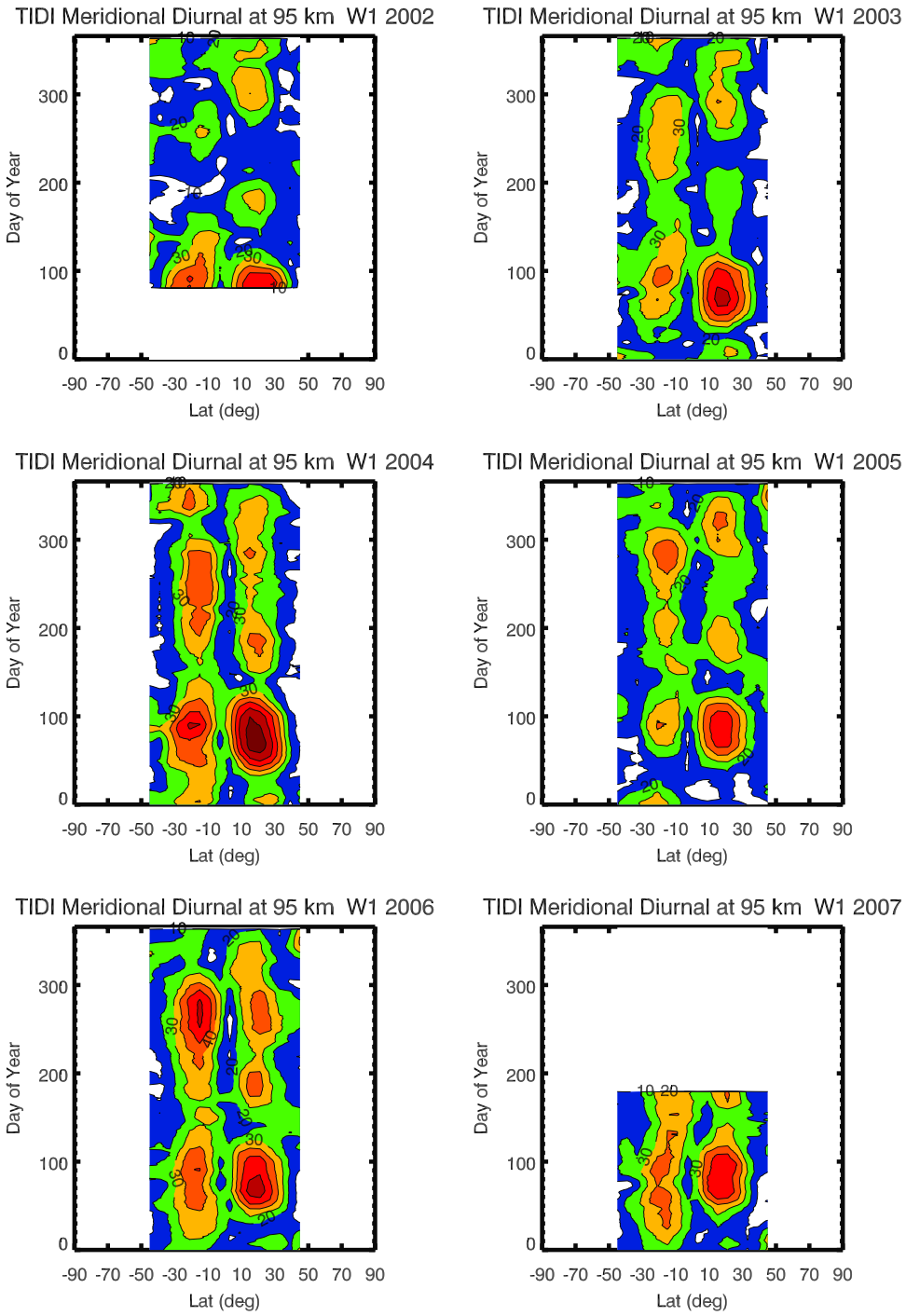

Figure 4b. TIDI migrating diurnal tide (W1) in meridional winds at 95 km. This plot shows the latitudinal and seasonal variations of meridional migrating diurnal tide at 95 km for all 6 years. The contour step is 10 m/s.

when the equatorial mesospheric mean zonal winds are westward (eastward) [*Hagan et al.*, 1999b, *Mayr and Mengel*, 2005]. Nevertheless, it has been difficult to determine the causal relationship between the tidal amplitude variations and the mean zonal winds. *Hagan et al.* [1999b] used the observed mean zonal winds to simulate the tidal variations and obtained the opposite effect on the tidal amplitude using GSWM, whereas *McLandress* [2002] obtained consistent migrating diurnal tide amplitude with observed mean zonal winds. *McLandress* [2002] attributed the tidal amplitude increase to the increase of the meridional gradient in the mean zonal winds. *Mayr and Mengel* [2005] suggested that the vertical gradient in the mean zonal wind could also be important in modulating the diurnal tide.

[7] It has been shown that gravity-wave-filtering variation due to the stratospheric QBO of zonal winds can generate a QBO with opposite phase in the mesospheric zonal winds [*Mayr et al.*, 1997]. *Lieberman* [1997] also

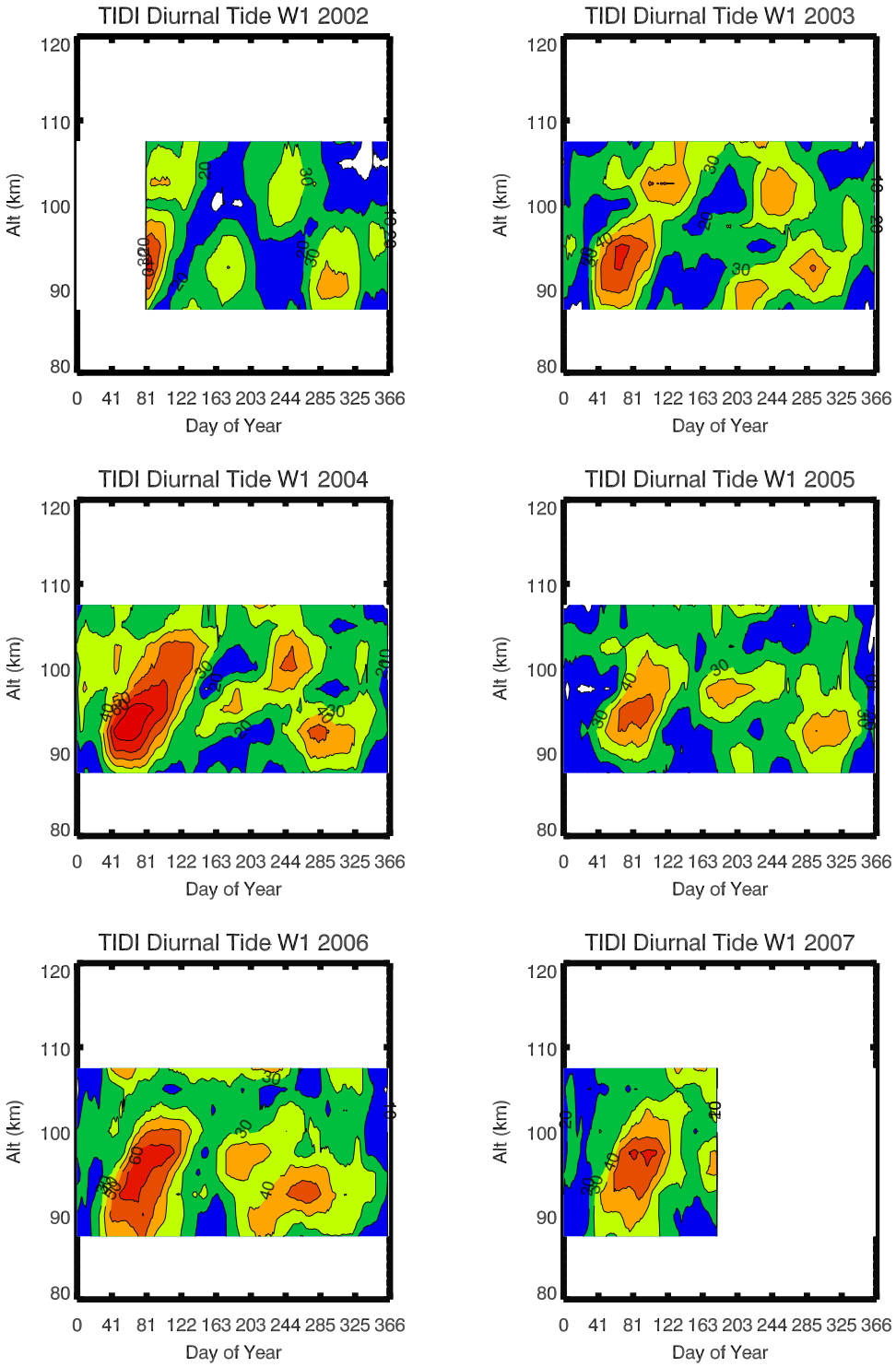

Figure 4c. TIDI migrating diurnal tide (W1) in meridional winds at 21 N. This plot shows the altitude and seasonal variations of meridional wind diurnal tide (W1) at 21°N. The contour step is 10 m/s.

suggested that the momentum flux of the migrating diurnal tide (1, 1) mode contributes to the maintenance of time-mean westward winds in the 90–105 km range. Perhaps, the momentum flux from the (1, 1) mode may also be partly responsible for the QBO related variations in the westward winds. Obviously, the QBO alters the gravity wave filtering pattern and leads to QBO-related variations in the migrating diurnal tide and mean zonal winds at high altitudes. Gravity waves may modulate the tidal amplitude directly or indirectly through the mean zonal winds. It may also be possible that gravity waves interact with the mean zonal wind indirectly through the tide. Thus, it is unclear that the interaction between the tidal amplitude and mean zonal winds is one way or two way. It will require observations and model simulation to resolve these issues.

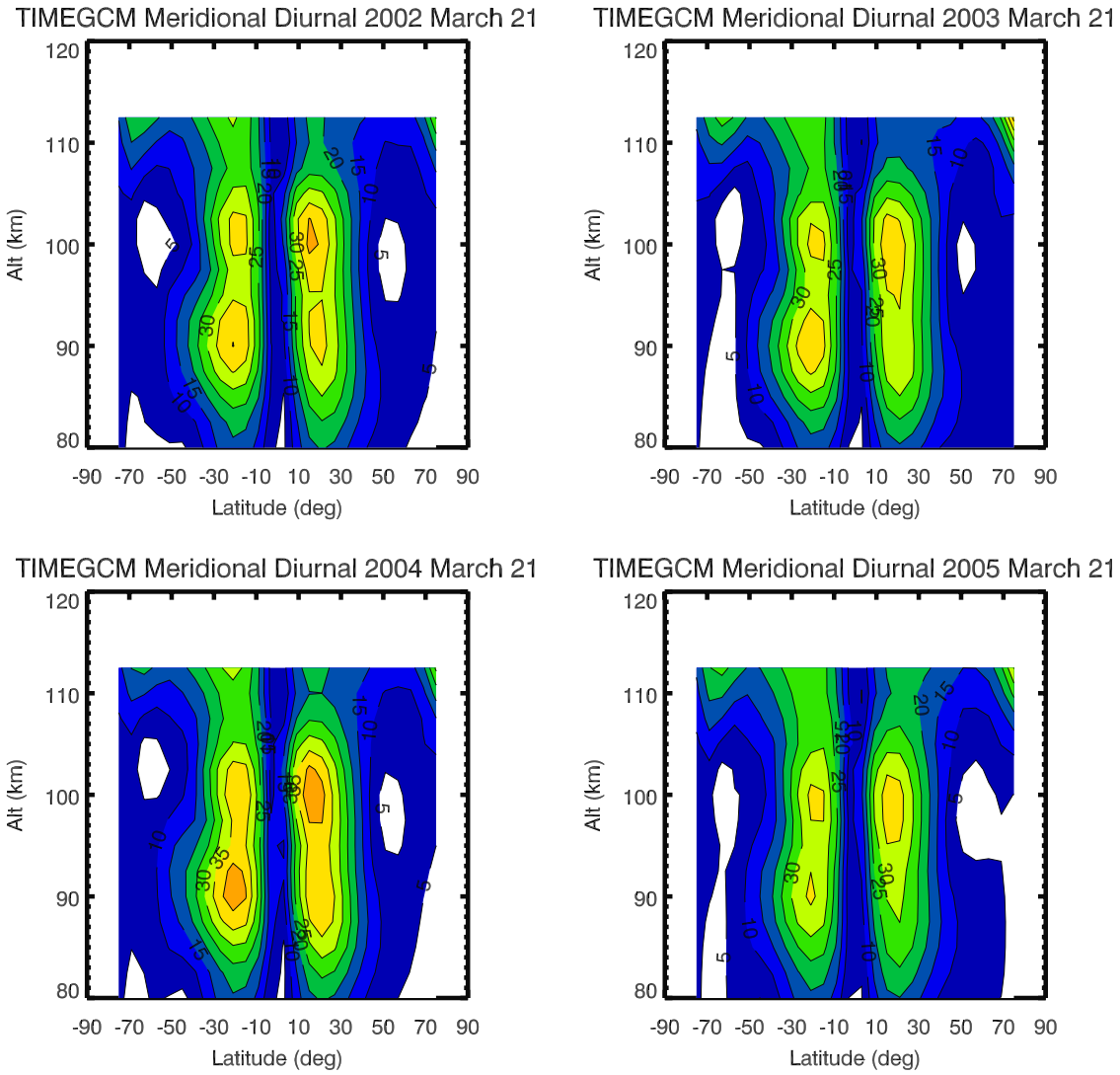

Figure 5a. TIMEGCM migrating diurnal tide W1 in meridional winds during the March equinox. Similar to Figure 4a for the TIMEGCM results at the TIDI sampling points during the 4 years. The contour step is 5 m/s.

[8] In this paper, we use recent mesospheric neutral wind data (from 2002 to 2007) from the TIMED instrument TIDI, in combination with the NCAR TIME-GCM 1.2 model annual run results (from 2002 to 2005) to examine the QBO effect on the migrating diurnal tide and mean zonal winds. In a companion paper [*Wu et al.*, 2008, hereinafter referred to as Part II], we will examine the QBO effect on the nonmigrating diurnal tides. We hope to shed some light on this very complex relationship between the diurnal amplitude and mean zonal winds under the influence of the QBO.

[9] Since its launch on 7 December 2001, the TIMED satellite has been in orbit for over 5 years. The TIDI instrument is a new generation of spaceborne interferometer, and it provides wider latitudinal and nighttime altitudinal coverage compared to the UARS HRDI instrument. Furthermore, TIDI is a dedicated mesospheric and lower thermospheric instrument with more complete and consistent coverage of the MLT region. Because of the 24-h local time coverage, the mean zonal wind results are less likely to be affected by the diurnal tide aliasing. Of course, the 24-h local time coverage is achieved by combining data sampled over 60 d.

[10] We also sampled the TIME-GCM 1.2 [*Roble and Ridley*, 1994] annual run at the TIDI data points and analyzed the TIME-GCM 1.2 results in the same manner. In this way, we eliminated any differences between the observations and the model due to sampling differences. The TIME-GCM 1.2 model is driven by the NCEP data (winds and temperature) at 10 hPa (roughly 30 km). Even though the TIME-GCM does not have an explicit QBO, the NCEP data will contain its effect, particularly in the stratospheric neutral winds. These QBO signatures, in turn, may manifest into the mesospheric and lower thermospheric region. We will study the interaction between the diurnal tide and mean zonal winds. This is probably the first attempt to use the TIME-GCM to study interannual variations originated from the lower boundary.

[11] The paper is organized as follows. In section 1, we give a brief description of the stratospheric environment for

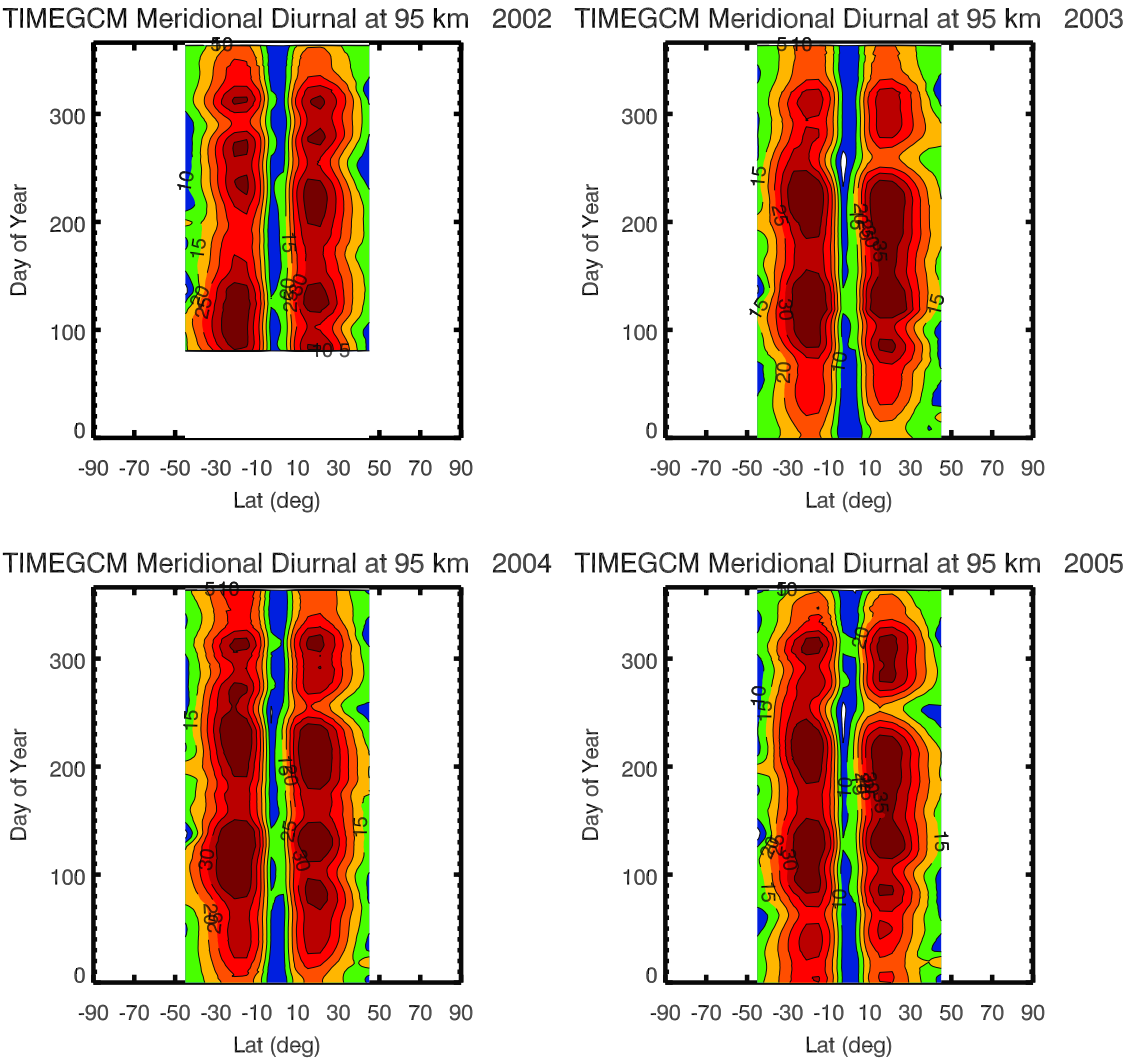

Figure 5b. TIMEGCM migrating diurnal tide W1 in meridional winds at 95 km. Similar to Figure 4b for the TIMEGCM results during the 4 years. The plot uses a contour step of 5 m/s.

the time period of interest, with information about the instrument. section 2 describes data analysis method. Section 3 shows the analysis results of the migrating diurnal tide in both the meridional and zonal winds. Section 4 is devoted to the mean zonal winds. We discuss the results in section 5 and summarize our findings in the section 6.

2. TIDI Data

2.1. Background Information

[12] TIDI data from 2002 d 051 (20 February) to the middle of 2007 are used in the study. Over that period, the stratospheric zonal winds experienced close to three QBO cycles. Figure 1 shows the monthly stratosphere zonal wind over Singapore from 2002 to 2007 (http://hyperion.gsfc.nasa.gov/Data_services/met/plots.html). The data are provided by Paul A. Newman of GSFC. The QBO cycles are apparent. During the years 2002, 2004, and 2006, the stratospheric zonal winds are in the eastward phase, while during 2003, 2005, and 2007 they are in the westward phase. The westward phase winds are usually stronger than those that occur during the eastward phase.

2.2. Brief Instrument Description and Data Sampling Distribution

[13] The TIDI instrument is a limb-scan Fabry-Perot interferometer, which monitors the Doppler shift in the airglow emissions caused by the neutral winds. The details of the instrument can be found in papers by *Killeen et al.* [1999, 2006] and *Skinner et al.* [2003]. In short, the instrument samples neutral winds on two sides of the satellite track; while one sampling track reaches the North Pole, the other flies over the South Pole. Because the TIMED satellite precesses slowly in local time (3 deg/day) or 12 h in 60 d, the local time of the sampling points does not change much during a day. However, the satellite has ascending and descending nodes, which are separated by close to 10 h. Therefore, the satellite can cover 24 h in local time for every 60 d with combined ascending and descending node data. The satellite orbits the Earth 15 times per day. Figure 2 plots the local times and latitudes of TIDI samples for the day 80 of

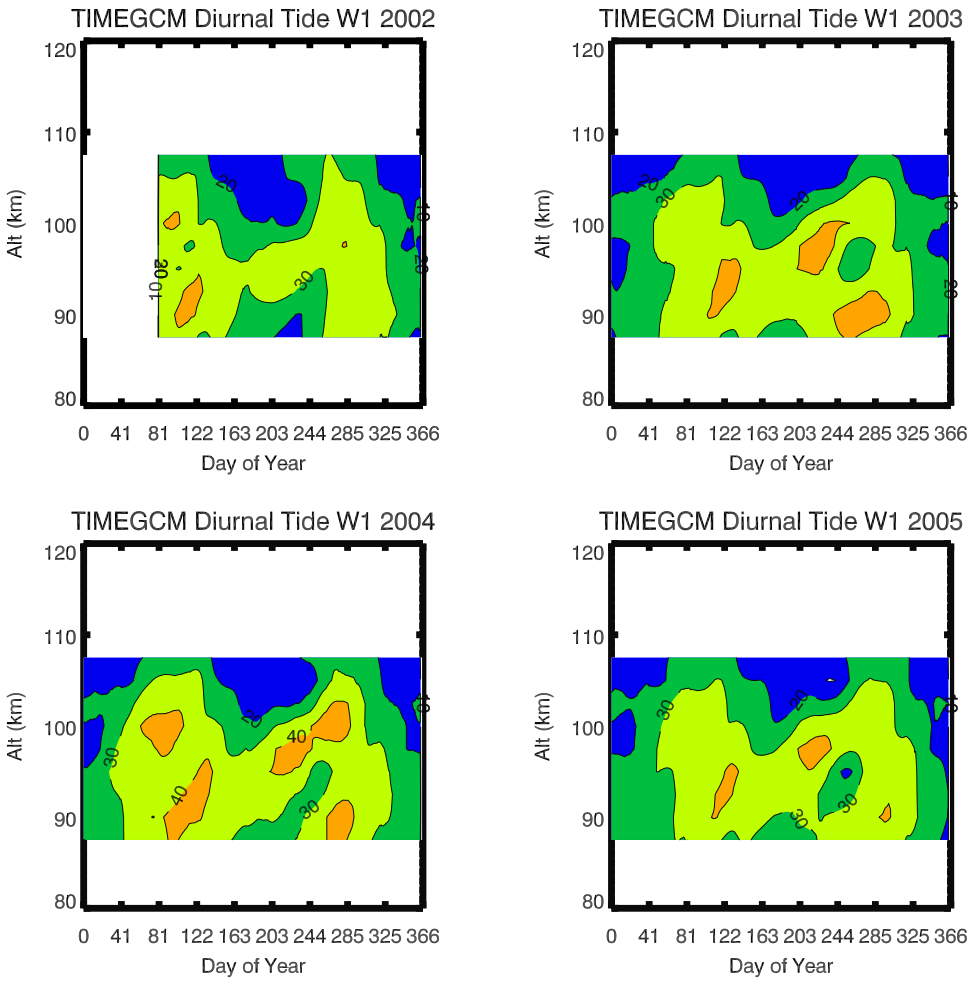

Figure 5c. TIMEGCM migrating diurnal tide W1 in meridional winds at 21°N. Similar to Figure 4c for the TIMECM results during the 4 years. This plot uses a contour step of 10 m/s.

2004 (20 March 2004). The red track goes to the North Pole (northern track) and the blue track (southern track) passes over the South Pole. The solid dots are for the daytime and hollowed dots for the nighttime. In a day, the whole sampling pattern will go over the Earth 15 times above different longitudes without drifting much in local time. Over a 60-d period, the whole sampling pattern will shift in local time by 12 h. The sampling region does overlap: Because both sides make measurements between 60°S and 60°N, there is coverage at four local times in this region. Outside this latitude region, the coverage is limited to one track with two local times. This coverage difference will have an impact on the precision of the tidal analysis; as we will show later on. In the vertical direction, the TIDI instrument scans from 70 to 115 km during the day and 80 to 105 km during the night. We selected the wind data from 85 to 107.5 km in our analysis, the data values at these lower and higher boundaries tend to have larger uncertainties due to the lack of airglow emission from these heights. We used the NCAR-processed O_2 ($^1\Sigma$) atmospheric band (0–0) P9 line (763.51 nm) TIDI data (version 0307). Specifically, TIDI filter 1–2 [*Killeen et al.*, 1999, Table 8] was used for the data acquisition. This version (0307) of P9 line data is available online with a new zero wind implementation. More details about NCAR data are provided by *Killeen et al.* [2006].

3. Data Analysis Method

[14] Because of TIDI's limited local time coverage during a day, it is impossible to calculate the daily tidal amplitude and phase without making assumptions about the latitudinal and vertical variations of the tide. One can obtain daily variations of the diurnal and semidiurnal tides by assuming that tides have only the most dominant Hough modes [*Hays et al.*, 1994; *Lieberman and Hays*, 1994]. If fast temporal variations are not the main concern, then one can also calculate tidal amplitudes and phases at different altitudes and latitude based on data from a 60-d window, which will provide a 24-h local time coverage. In this approach, one need not assume anything about the latitudinal and vertical variations. However, the result will be an average representation over a 60-d period. Since we mainly concern about seasonal, annual, and interannual variations, we analyze the TIDI data based on a 60-d sliding window using *Wu et al.* [1995] least squares method for space-time spectral analysis. This spectral method has also been used to extract the quasi-two day wave from the TIDI data [*Limpasuvan et al.*,

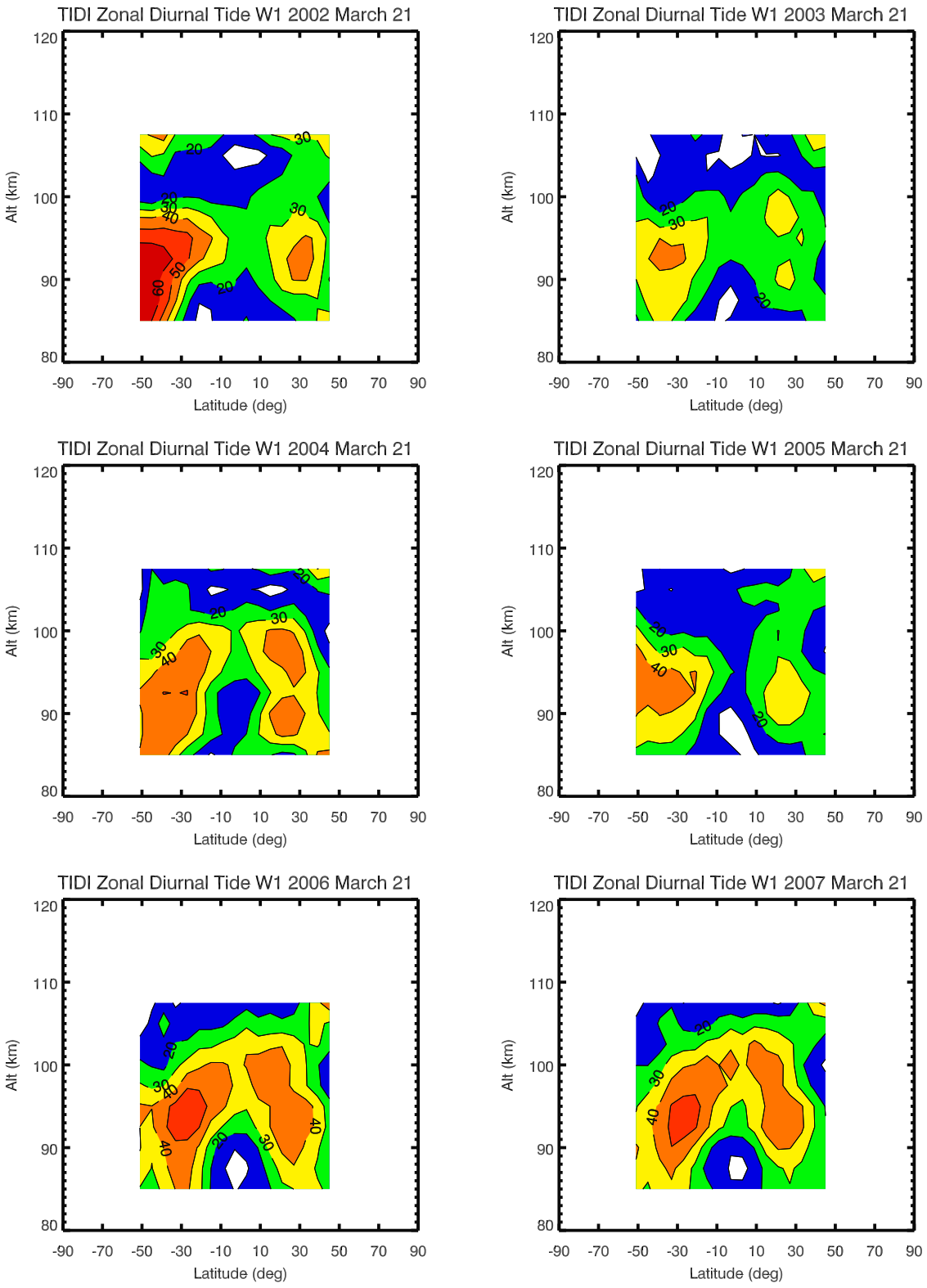

Figure 6a. TIDI migrating diurnal tide W1 in zonal winds during the March equinox. The March equinox altitude and latitude variations of the zonal wind migrating diurnal tide amplitude are plotted. The contour step is 10 m/s.

2005]. We performed the space-time series spectral analysis to the southern and northern tracks separately, to obtain tidal amplitudes and phases of migrating and nonmigrating tides. We then combined the results from the southern and northern tracks to form a global view of the tidal amplitudes and phases. The final result has a horizontal resolution of 6 degrees in latitude and a vertical resolution of 2.5 km.

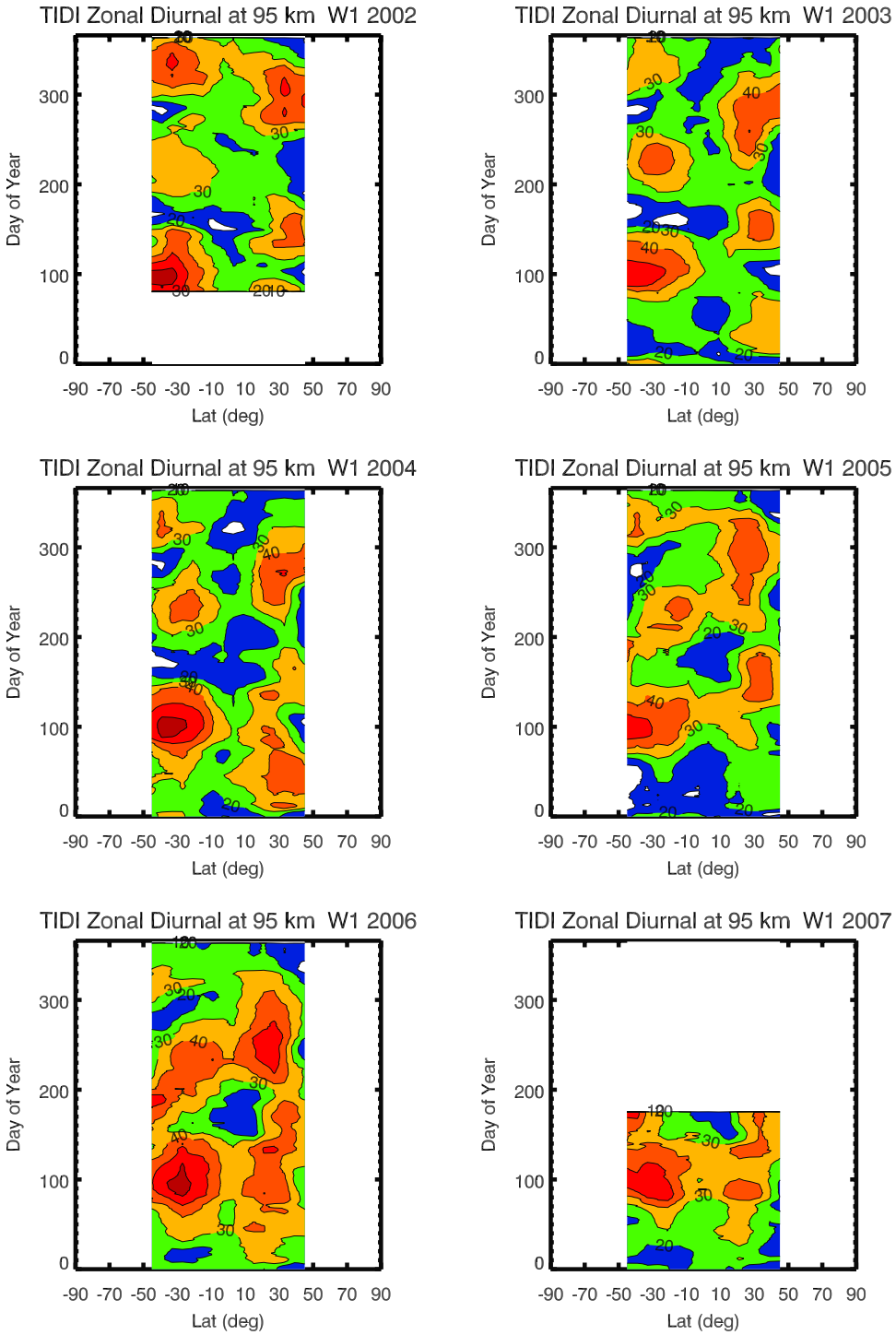

Figure 6b. TIDI migrating diurnal tide W1 in zonal winds at 95 km. The latitudinal and seasonal changes at 95 km are plotted. The contour step is 10 m/s.

[15] On the basis of the precision of the wind measurements, which is determined by photon count statistics, we estimate the precision of the tidal amplitude calculation during the March equinox of each of the 6 years (2002–2007). The results are shown in Figure 3. The precision improved from 2002 to 2005 due to the reduction of ice on TIDI optics through two roll maneuvers in 2003 and gradual sublimation over the years [*Skinner et al.*, 2003]. Beyond 2005, the precision did not vary much. The vertical variations are mostly due to the O_2 (0–0) band airglow emission profile. The O_2 (0–0) band peaks near 94 km; consequently, the wind error is smallest at that height. Above 105 km, only daytime data are available, and thus, the error increases. The latitudinal variations are caused by the distribution of the sampling point. Both the southern and northern tracks cover the region between 60°S and 60°N latitudes, resulting in more data points and smaller statistical errors. In the high-latitude regions (>60 degrees latitude),

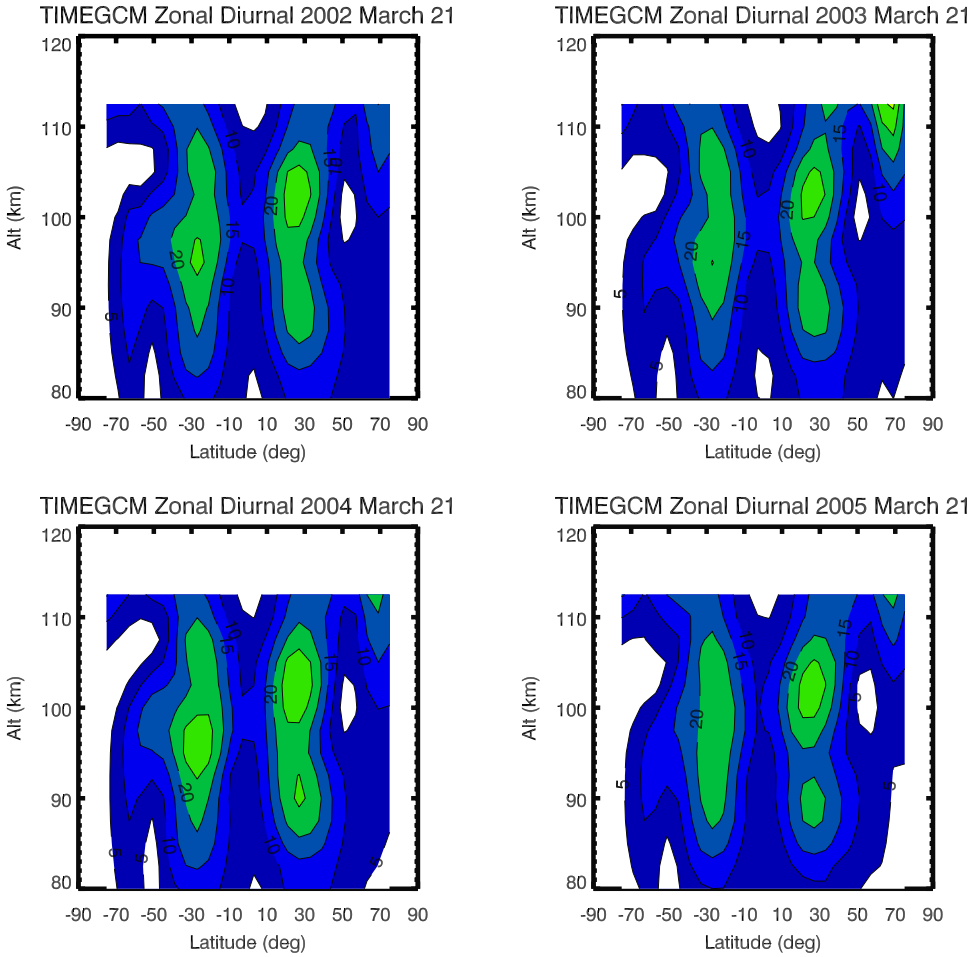

Figure 7a. TIMEGCM migrating diurnal tide W1 in zonal winds during the March equinox. Similar to Figure 6a for the TIMEGCM zonal winds during the 4 years. The contour step is 5 m/s.

only one track passes over, having fewer sampling points that causes higher statistical errors. While it is easier to compute statistical errors, systematic errors are much difficult to ascertain. Hence, the tidal amplitudes may contain some systematic biases, which will gradually lessen with an improvement of data in the future. At this point, it appears that we still have some noticeable bias at high latitude region affecting the migrating tide analysis. For that reason, we limit our discussion to midlatitude and low-latitude regions for the migrating tide results. Because of high precision, the results should provide mostly reliable relative changes for interannual comparisons.

4. Diurnal Tide in Mesospheric Winds

4.1. Migrating Diurnal Tide in Meridional Winds

4.1.1. TIDI Results

[16] The migrating tide amplitudes of meridional winds for each season during the six years from 2002 to 2007 are plotted in Figure 4. To highlight the interannual variations we plotted the same seasons of different years side by side. Figure 4a is for the March equinox. The time period of 60 d centers at day 81 (21 March). The years on the left side (2002, 2004, and 2006) show the eastward phase of the stratospheric QBO. The right side (2003, 2005, and 2007) shows the westward phase. The contrast between the left and right sides is quite apparent, while the difference between the years 2006 and 2007 appears to be smaller. Stronger diurnal tide amplitudes are observed during the eastward phase of the stratospheric QBO. Besides the interannual variations, interhemispheric differences are also quite noticeable. The amplitude peak altitudes in the two hemispheres have offset in height and those in the southern hemisphere tend to have double peaks. The large tidal amplitudes at northern high latitude and high altitudes appear to be a result of bias in the winds, which tends to affect the migrating tide results. For this reason, we have limited our analysis of the migrating tide to 50 degrees latitude. To examine the seasonal variation, Figure 4b shows the tidal amplitude variations at 95 km for each of the 6 years. The vertical coordinate marks the center of the 60-d sliding window in which we performed the space-time series spectral analysis. The first 2002 60-d sliding window centers at day 81 (21 March 2002). Peaks at March and September equinoxes are visible. The March equinox diurnal tide amplitudes are larger during 2002, 2004, and 2006 than in other years. Because of the late start in the data set, the increase in 2002 is not as obvious as that in 2004. The amplitude in the northern hemisphere shows consistent larger values than the amplitude in the southern hemisphere. Figure 4c displays the diurnal tide amplitude at

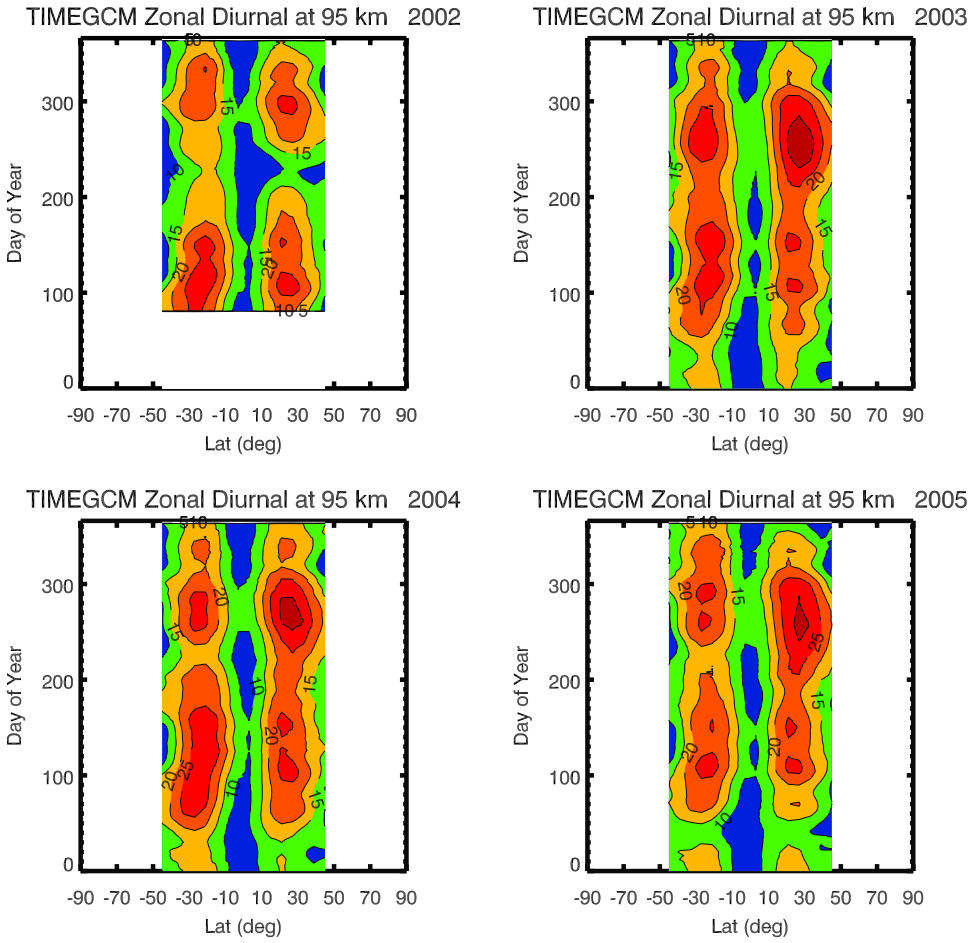

Figure 7b. TIMEGCM migrating diurnal tide W1 in zonal winds at 95 km. Similar to Figure 6b for the TIMEGCM zonal winds during the 4 years. The contour step is 5 m/s.

21°N for the 6 years. The March equinox maximum is apparent for all years. The amplitude of the migrating diurnal tide appears to shift upward during the March equinox for all years. Again because of the late start of the 2002 data, the slight increase in the 2002 March equinox is not clearly seen. We should note that the starting point of 2002 is day 81 (21 March). On that day we still see the contour of 60 m/s. In 2003, the same 60 m/s contour line did not appear to extend to day 81 (21 March). The increases in 2004 and 2006 are very obvious. There is no clear QBO-related variation for the September equinox peaks.

4.1.2. TIME-GCM Results

[17] Figure 5a shows the March equinox results from the TIME-GCM annual run (2002–2005). There is a very small increase in the tide amplitude during the eastward phase (2002 and 2004). Both hemispheres show multiple peaks at similar heights with varying amplitudes. The amplitudes are in general smaller than those from the TIDI observations. Figure 5b shows the migrating diurnal tide amplitude at 95 km. We can hardly identify the increase during the March equinox. Figure 5c illustrates the diurnal tide amplitude at 21°N. The March equinox amplitude in 2002 is only slightly larger than those in 2003 and 2005 (Figure 4a) noting the small 40 m/s contour line near 100 km, but the increase is more obvious in 2004. The peak amplitude also appears to shift upward during the March equinox for all 4 years.

4.2. Migrating Diurnal Tide in Zonal Winds

4.2.1. TIDI Results

[18] Figure 6a illustrates the March equinox zonal wind diurnal amplitudes. The zonal diurnal tide tends to peak around 30°N and 30°S; we note that the meridional diurnal tide peaks at 20°N and 20°S. In the southern hemisphere, the peak amplitude is much more widely distributed into the midlatitude region (50°N). We also see a tendency to have larger amplitudes during the eastward phase of the stratospheric QBO (2002 and 2004). The differences between 2006 and 2007 are smaller. The amplitude at 95 km also shows large March equinox peaks during 2002, 2004, and 2006 in the southern hemisphere (Figure 6b).

4.2.2. TIME-GCM Results

[19] The March equinox amplitudes in the southern hemisphere are larger during the eastward phase of QBO (Figure 7a). The zonal wind amplitude in general is smaller than that of the meridional winds. We also see peak height offsets between the two hemispheres. The amplitudes at 95 km are displayed in Figure 7b; the increase in the 2002 March equinox is less obvious. The March equinox amplitude in 2004 is larger, as shown by the larger area of the 25 m/s contour line. There is a September equinox peak during all 4 years, but no apparent QBO-related variation for the September equinox season. The TIME-GCM diurnal

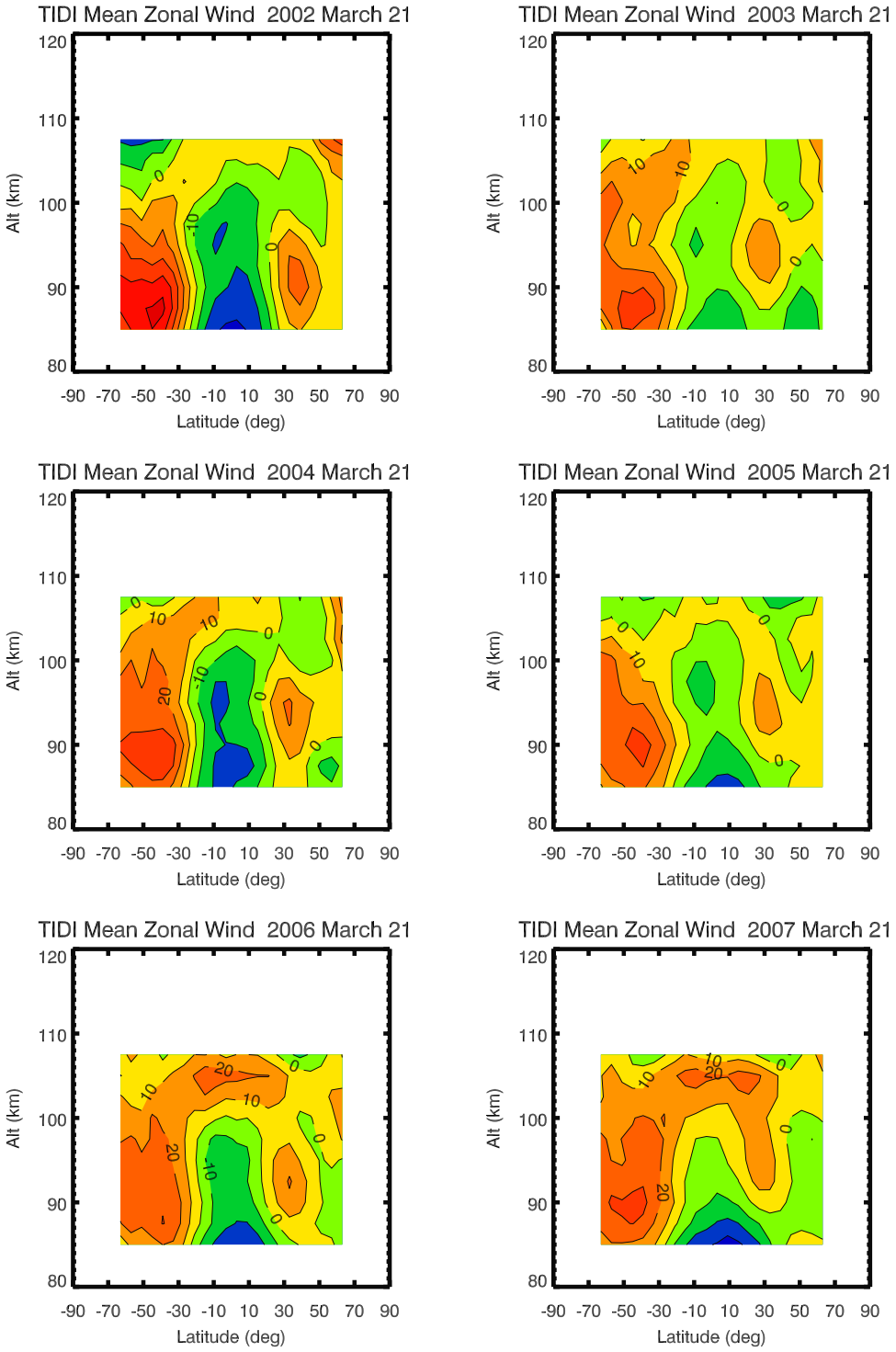

Figure 8. TIDI zonal mean winds. Mean zonal winds from 60-d slighting window for the March equinox season (centered on day 81, 21 March). The contour step is 10 m/s.

tide amplitudes range from 60 to 70 percent of those observed by the TIDI instrument.

5. Mean Zonal Winds

5.1. TIDI Results

[20] The mean zonal winds from a 60-d window during the March equinox are displayed in Figure 8. The distinction between the two phases of the QBO is very obvious. During the eastward phase of the QBO, there is a large region of westward zonal winds centered at the equator that extend to about 100 km, the westward zonal winds are smaller during the westward phase of the QBO. Enhancements of the eastward wind also appeared near 30°N and 40°S during the eastward phase of the QBO. Hence, there is a further increase of the meridional gradient of the mean zonal wind

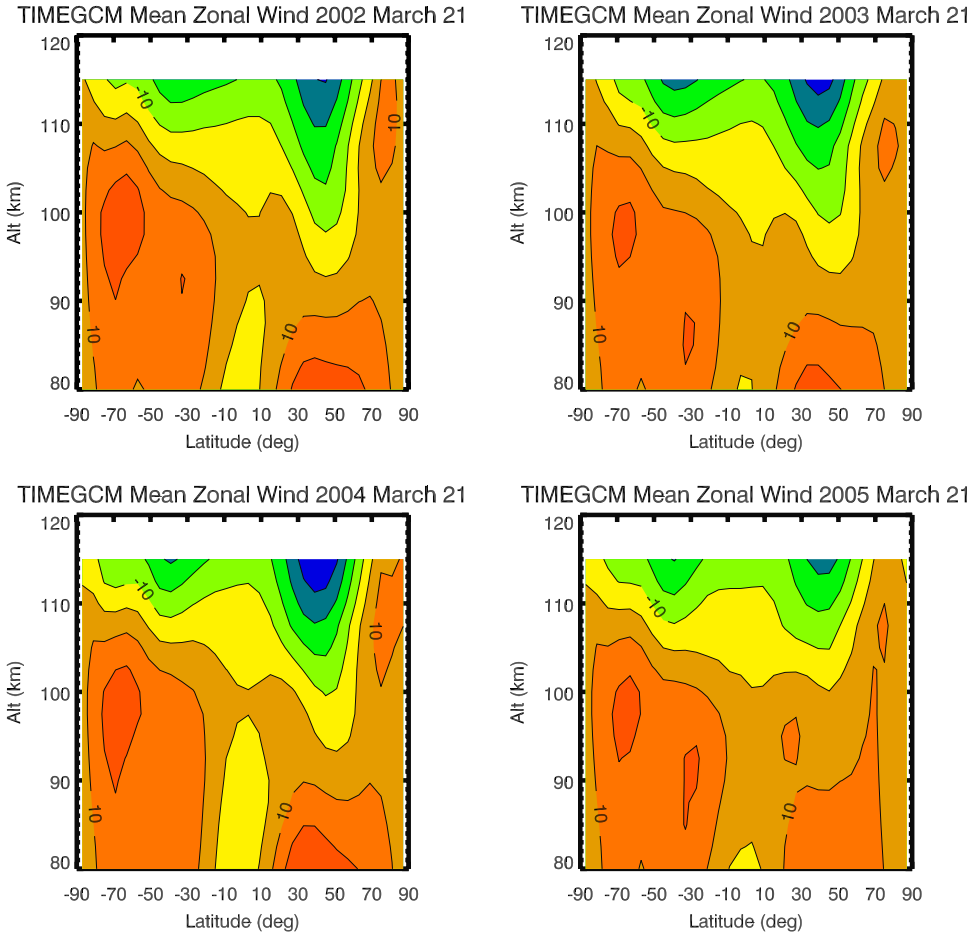

Figure 9. TIMEGCM zonal mean winds. Same as Figure 8 for the mean zonal winds from the TIME-GCM results during the 4 years. The contour step is 10 m/s.

during the eastward phase of the QBO. In 2002, there was a strong eastward wind region in the southern hemisphere. However, the contribution of the ice condensation on TIDI optics to the mean zonal wind results cannot be ruled out completely. We also notice that while the differences in the equatorial zonal mean winds between 2006 and 2007 are similar to that between 2004 and 2005, the equatorial zonal mean winds in 2006 and 2007 are less westward.

5.2. TIME-GCM Results

[21] The simulation from the NCAR TIME-GCM for the March equinox is shown in Figure 9. Even though the westward wind region is much weaker and smaller, it also appears during the eastward phase of the QBO, as TIDI observational results have shown. The large eastward region in the southern hemisphere is present, as in the case of the TIDI observations, though with smaller wind magnitude.

6. Discussions

6.1. March Equinox Season

[22] During the March equinox, we see a strong QBO dependence in TIDI data and TIME-GCM runs. The westward zonal winds at the equator coincide with the enhanced meridional and zonal wind migrating tide. To illustrate the connection between the mesospheric tidal amplitudes and stratospheric winds, from 2002 to 2007 we plot the diurnal tide amplitude at 20°N and 95 km altitude, the largest eastward winds and westward winds from the altitude range of Singapore monthly stratospheric wind data (Figure 10). The amplitude of the diurnal tide increases during the year when the difference between the largest eastward and westward winds is small (eastward phase of the QBO). When the winds are small in both the eastward and westward directions, we should expect the filtering of the gravity waves be small as well. The result suggests that as more gravity waves pass into the mesosphere, the tidal amplitude increases. We should also note that because the QBO is not exactly a 2-year oscillation, we see a shift of the smallest westward wind to a later date in 2006, which is further away from the March equinox. We speculate that may be the reason the QBO effect is smaller in 2006 and 2007.

[23] The TIME-GCM reproduces the QBO-related mean zonal wind variations observed by the TIDI, although to a lesser extent. At the same time the TIME-GCM diurnal tide increases during the eastward phase of the QBO is also smaller. Both the enhancements in the tide and the westward zonal wind region near the equator during the eastward phase of the QBO are generated by the TIME-GCM based on the NCEP data at 10 hPa, while the tidal amplitudes at 10 hPa from the GSWM remain the same for all 4 years. Compared to TIDI observations (~30 m/s), the TIME-GCM

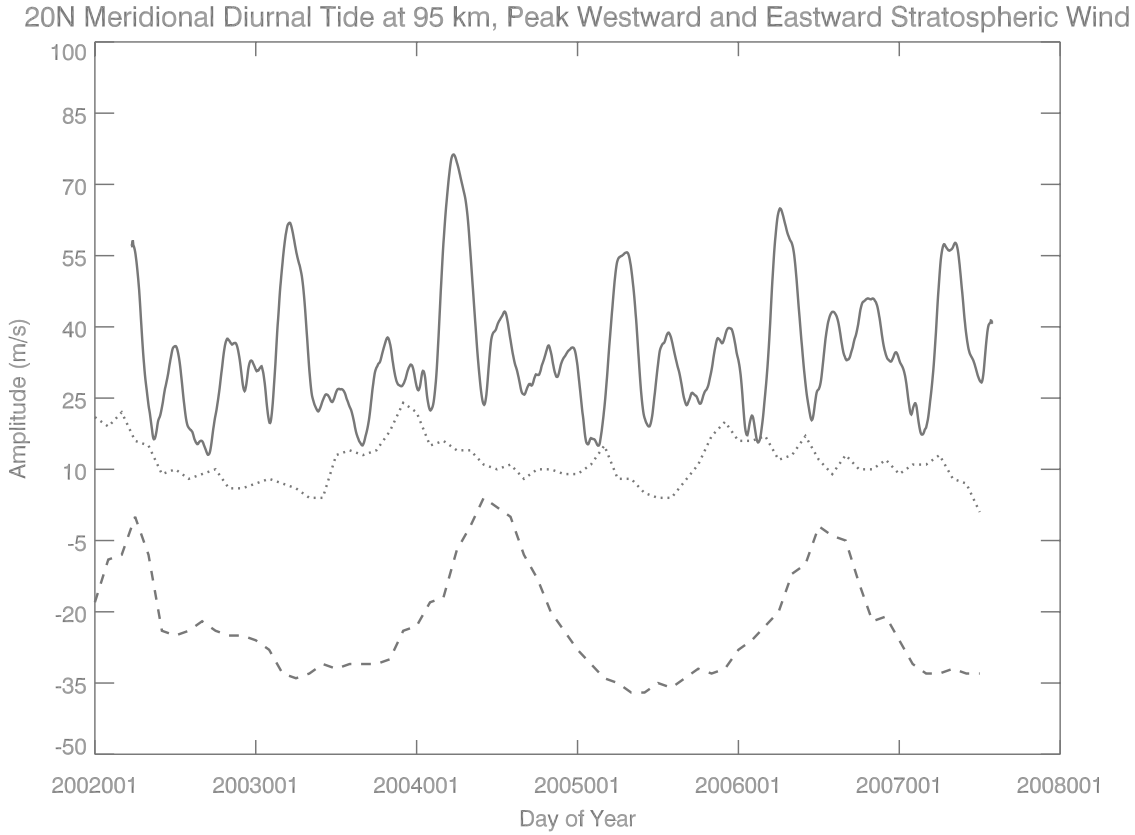

Figure 10. The 20°N meridional diurnal tide at 95 km and peak westward and eastward stratospheric winds. The migrating meridional diurnal tide amplitudes at 20°N and 95 km are plotted as a solid line. The peak stratospheric eastward winds are shown as a dotted line. The peak stratospheric westward winds are marked by a dashed line. The stratospheric wind results are based on Singapore monthly wind observations from 70 to 10 hPa shown in Figure 1.

mean westward winds near the equator are small (<10 m/s), as is the increase in the tide amplitude. The TIME-GCM tide amplitude is small in general, which is likely because the spatial resolution (half of the scale height in vertical and 5 × 5 degrees in horizontal) of the model is not sufficient for the migrating diurnal tide with a vertical wavelength of ~20 km. A new double resolution TIME-GCM 1.3 (under testing) is able to produce more comparable amplitude.

6.2. Tidal Amplitudes and Mean Zonal Winds

[24] The TIDI data show a strong connection between the tidal amplitude and the mean zonal winds associated with QBO as observed in the past by HRDI [*Hagan et al.*, 1999b]. Large tidal amplitude is observed when the westward zonal wind appears near the equator. The QBO effect on the mean zonal wind is not limited to the lower latitudes; we also noticed an increase of the eastward zonal wind in the midlatitudes during the eastward phase of QBO (March equinox).

6.3. Interhemispheric Asymmetry

[25] There is a large asymmetry in tidal amplitude. Moreover, the mean zonal wind also exhibits asymmetry between the two hemispheres even during the March equinox. The eastward wind in the southern midlatitudes is particularly strong during 2002 March equinox. The TIME-GCM results tend to be more symmetric in the tidal amplitude peak altitude location. The asymmetry in the model mean zonal wind has the same general features observed by the TIDI instrument.

7. Summary

[26] The TIDI data provide a global view of the meridional and zonal wind migrating diurnal tide and mean zonal winds. The data show strong seasonal variations of the migrating tide with the strongest amplitude in the March equinox. In addition, the migrating diurnal tide is strongly affected by the QBO, the strongest effect being in the March equinox when the diurnal tide peaks in a year. The QBO effect on the mean zonal wind appears to extend into the midlatitude region by increasing the eastward wind during the March equinox. The TIME-GCM driven by the NCEP data at 10 hPa is able to reproduce the QBO effect in the diurnal tide and mesospheric zonal wind, although to a lesser extent. Since the TIME-GCM is driven by tidal amplitudes from the GSWM output at 10 hPa without interannual variations, a small mesospheric QBO effect is expected. We expect to see the TIME-GCM produce even better agreement with observations in the future.

[27] **Acknowledgments.** This work is supported by a NASA grant NAG5–5334 to the National Center for Atmospheric Research and NAG5–5049 to the University of Michigan. NCAR is supported by the

National Science Foundation. This work is also supported in part by the Chinese Academy of Sciences International Partnership Program for Creative Research Teams.

[28] Amitava Bhattacharjee thanks the reviewers for their assistance in evaluating this paper.

References

Burrage, M. D., M. E. Hagan, W. R. Skinner, D. L. Wu, and P. B. Hays (1995), Long-term variability in the solar diurnal tide observed by HRDI and simulated by the GSWM, *Geophys. Res. Lett.*, *22*(19), 2641–2644, doi:10.1029/95GL02635.

Chapman, S., and R. S. Lindzen (1970), *Atmospheric Tides*, 200 pp., Gordon and Breach, Newark, N. J.

Forbes, J. M. (1982a), Atmospheric tides, 1, Model description and results for the solar diurnal component, *J. Geophys. Res.*, *87*(A7), 5222–5240, doi:10.1029/JA087iA07p05222.

Forbes, J. M. (1982b), Atmospheric tides, 2, The solar and lunar semidiurnal components, *J. Geophys. Res.*, *87*(A7), 5241–5252, doi:10.1029/JA087iA07p05241.

Forbes, J. M., and M. E. Hagan (1988), Diurnal propagating tide in the presence of mean winds and dissipation: A numerical investigation, *Planet. Space Sci.*, *36*, 579–590, doi:10.1016/0032-0633(88)90027-X.

Forbes, J. M., X. Zhang, E. R. Talaat, and W. Ward (2003a), Nonmigrating diurnal tides in the thermosphere, *J. Geophys. Res.*, *108*(A1), 1033, doi:10.1029/2002JA009262.

Forbes, J. M., M. E. Hagan, S. Miyahara, Y. Miyoshi, and X. Zhang (2003b), Diurnal nonmigrating tides in the tropical lower thermosphere, *Earth Planets Space*, *55*, 419–426.

Hagan, M. E., and J. M. Forbes (2002), Migrating and nonmigrating diurnal tides in the middle and upper atmosphere excited by tropospheric latent heat release, *J. Geophys. Res.*, *107*(D24), 4754, doi:10.1029/2001JD001236.

Hagan, M. E., and J. M. Forbes (2003), Migrating and nonmigrating semidiurnal tides in the upper atmosphere excited by tropospheric latent heat release, *J. Geophys. Res.*, *108*(A2), 1062, doi:10.1029/2002JA009466.

Hagan, M. E., M. D. Burrage, J. M. Forbes, J. Hackney, W. J. Randel, and X. Zhang (1999a), GSWM-98: Results for migrating solar tides, *J. Geophys. Res.*, *104*(A4), 6813–6827, doi:10.1029/1998JA900125.

Hagan, M. E., M. D. Burrage, J. M. Forbes, J. Hackney, W. J. Randel, and X. Zhang (1999b), QBO effects on the diurnal tide in the upper atmosphere, *Earth Planets Space*, *51*, 571–578.

Hays, P. B., D. L. Wu, M. D. Burrage, D. A. Gell, H. J. Grassl, R. S. Lieberman, A. R. Marshall, Y. T. Morton, D. A. Ortland, and W. R. Skinner (1994), Observations of the diurnal tide from space, *J. Atmos. Sci.*, *51*, 3077–3093, doi:10.1175/1520-0469(1994)051<3077:OOTDTF>2.0.CO;2.

Huang, F. T., and C. A. Reber (2004), Nonmigrating semidiurnal and diurnal tides at 95 km based on wind measurements from the High Resolution Doppler Imager on UARS, *J. Geophys. Res.*, *109*, D10110, doi:10.1029/2003JD004442.

Huang, F. T., H. G. Mayr, C. A. Reber, J. M. Russell, M. Mlynczak, and J. G. Mengel (2006), Stratospheric and meosphereic temperature variations for the quasi-biennial and semiannual (QBO and SAO) oscillations based on measurements from SABER (TIMED) and MLS (UARS), *Ann. Geophys.*, *24*, 2131–2149.

Khattatov, B. V., V. A. Yubin, M. A. Geller, P. B. Hays, and R. A. Vincent (1997a), Diurnal migrating tide as seen by the high resolution Doppler imager/UARS 1. Monthly mean global meridional winds, *J. Geophys. Res.*, *102*(D4), 4405–4422, doi:10.1029/96JD03655.

Khattatov, B. V., M. A. Geller, V. A. Yubin, and P. B. Hays (1997b), Diurnal migrating tide as seen by the high resolution Doppler imager/UARS 2. Monthly mean global zonal and vertical velocities, pressure, temperature, and inferred dissipation, *J. Geophys. Res.*, *102*(D4), 4423–4435, doi:10.1029/96JD03654.

Killeen, T. L., et al. (1999), TIMED Doppler Interferometer (TIDI), in *Optical Spectroscopic Techniques and Instrumentation for Atmospheric and Space Research*, vol. 3, edited by A. M. Larar, *Proc. SPIE*, *3756*, 289–301.

Killeen, T. L., Q. Wu, S. C. Solomon, D. A. Ortland, W. R. Skinner, and R. J. Niciejewski (2006), TIMED Doppler Interfereometer: Overview and recent results, *J. Geophys. Res.*, *111*, A10S01, doi:10.1029/2005JA011484.

Lieberman, R. (1997), Long-term variations of zonal mean winds and (1,1) driving in the equatorial lower thermosphere, *J. Atmos. Sol. Terr. Phys.*, *59*, 1483–1490, doi:10.1016/S1364-6826(96)00150-2.

Lieberman, R. S., and P. B. Hays (1994), An estimate of the momentum deposition in the lower thermosphere by the observed diurnal tide, *J. Atmos. Sci.*, *51*, 3094–3105, doi:10.1175/1520-0469(1994)051<3094:AEOTMD>2.0.CO;2.

Limpasuvan, V., D. L. Wu, M. J. Schwartz, J. W. Waters, Q. Wu, and T. L. Killeen (2005), The two-day wave in EOS MLS temperature and wind measurements during 2004–2005 winter, *Geophys. Res. Lett.*, *32*, L17809, doi:10.1029/2005GL023396.

Manson, A. H., C. E. Meek, S. K. Avery, and D. Tetenbaum (1988), Comparison of mean wind and tidal fields at Saskatoon (52°N, 107°W) and Poker Flat (65°N, 147°W) during 1983/1984, *Phys. Scr.*, *37*, 169–177, doi:10.1088/0031-8949/37/1/027.

Manson, A. H., C. E. Meek, H. Teitelbaum, F. Vial, R. Schminder, D. Kurschner, M. J. Smith, G. J. Fraser, and R. R. Clark (1989), Climatologies of semi-diurnal and diurnal tides in the middle atmosphere (70–110 km) at middle latitudes (40–55 degrees), *J. Atmos. Sol. Terr. Phys.*, *51*, 579–593, doi:10.1016/0021-9169(89)90056-1.

Manson, A. H., et al. (1999), Seasonal variations of the semi-diurnal and diurnal tides in the MLT: Multi-year MF radar observations from 2–70°N, and the GSWM tidal model, *J. Atmos. Sol. Terr. Phys.*, *61*, 809–828, doi:10.1016/S1364-6826(99)00045-0.

Mayr, H. G., and J. G. Mengel (2005), Interannual variations of the diurnal tide in the mesosphere generated by the quasi-biennial oscillation, *J. Geophys. Res.*, *110*, D10111, doi:10.1029/2004JD005055.

Mayr, H. G., J. G. Mengel, C. O. Hines, K. L. Chan, N. F. Arnold, C. A. Reddy, and H. S. Porter (1997), The gravity wave Doppler spread theory applied in a numerical spectral model of the middle atmosphere: 2. Equatorial oscillations, *J. Geophys. Res.*, *102*(D22), 26,093–26,105, doi:10.1029/96JD03214.

McLandress, C. (2002), Interannual variations of the diurnal tide in the mesosphere induced by a zonal-mean wind oscillation in the tropics, *Geophys. Res. Lett.*, *29*(9), 1305, doi:10.1029/2001GL014551.

McLandress, C., Y. Rochon, G. G. Shepherd, B. H. Solheim, G. Thuillier, and F. Vial (1994), The meridional wind component of the thermospheric tide observed by WINDII on UARS, *Geophys. Res. Lett.*, *21*, 2417–2420.

McLandress, C., G. G. Shepherd, and B. H. Solheim (1996), Satellite observations of thermospheric tides: Results from the Wind Imaging interferometer on UARS, *J. Geophys. Res.*, *101*(D2), 4093–4114, doi:10.1029/95JD03359.

Morton, Y. T., R. S. Lieberman, P. B. Hays, D. A. Ortland, A. R. Marshell, D. L. Wu, W. R. Skinner, M. D. Burrage, D. A. Gell, and J.-H. Yee (1993), Global mesospheric tidal winds observed by the high resolution research satellite, *Geophys. Res. Lett.*, *20*(12), 1263–1266, doi:10.1029/93GL00826.

Oberheide, J., Q. Wu, D. A. Ortland, T. L. Killeen, M. E. Hagan, and R. G. Roble (2005), Nonmigrating diurnal tides as measured by the TIMED Doppler Interferometer: Preliminary results, *Adv. Space Res.*, *35*(11), 1911–1917, doi:10.1016/j.asr.2005.01.063.

Oberheide, J., Q. Wu, T. L. Killeen, M. E. Hagan, and R. G. Roble (2006), Diurnal nonmigrating tides from TIDI wind data: Monthly climatologies and seasonal variations, *J. Geophys. Res.*, *111*, A10S03, doi:10.1029/2005JA011491.

Pancheva, D., et al. (2002), Global-scale tidal variability during the PSMOS campaign of June–August 1999: Interaction with planetary waves, *J. Atmos. Sol. Terr. Phys.*, *64*, 1865–1896, doi:10.1016/S1364-6826(02)00199-2.

Roble, R. G., and E. C. Ridley (1994), A thermosphere-ionosphere-mesosphere-electrodynamics general circulation model (time-GCM): Equinox solar cycle minimum simulations (30–500 km), *Geophys. Res. Lett.*, *21*(6), 417–420, doi:10.1029/93GL03391.

She, C. Y., et al. (2004), Tidal perturbations and variability in the mesopause region over Fort Collins, CO (41N, 105W): Continuous multi-day temperature and wind lidar observations, *Geophys. Res. Lett.*, *31*, L24111, doi:10.1029/2004GL021165.

Skinner, W. R., et al. (2003), Operational performance of the TIMED Doppler Interferometer (TIDI), in *SPIE Annual Meeting 2003: Remote Sensing and Space Technology (Special Collection)*, edited by A. M. Larar, J. A. Shaw, and Z. Sun, *Proc. SPIE*, *5157*, 47–57, doi:10.1117/12.503727.

Vial, F. (1989), Tides in the middle atmosphere, *J. Atmos. Terr. Phys.*, *51*, 3–17, doi:10.1016/0021-9169(89)90069-X.

Vincent, R., A. S. Kovalam, D. D. Fritts, and J. R. Isler (1998), Long-term MF radar observations of solar tide in the low-latitude mesosphere: Interannual variability and comparison with the GSWM, *J. Geophys. Res.*, *103*(D8), 8667–8684, doi:10.1029/98JD00482.

Wu, D. L., P. B. Hays, and W. R. Skinner (1995), A least squares method for spectral analysis of space-time series, *J. Atmos. Sci.*, *52*, 3501–3511, doi:10.1175/1520-0469(1995)052<3501:ALSMFS>2.0.CO;2.

Wu, Q., T. L. Killeen, D. A. Ortland, S. C. Solomon, R. D. Gablehouse, R. M. Johnson, W. R. Skinner, R. J. Niciejewski, and S. J. Franke (2006), TIMED Doppler Interferometer (TIDI) observations of migrating diurnal

and semi-diurnal tides, *J. Atmos. Sol. Terr. Phys.*, *68*, 408–417, doi:10.1016/j.jastp.2005.02.031.

Wu, Q., D. A. Ortland, T. L. Killeen, R. G. Roble, M. E. Hagan, H.-L. Liu, S. C. Solomon, J. Xu, W. R. Skinner, and R. J. Niciejewski (2008), Global distribution and interannual variations of mesospheric and lower thermospheric neutral wind diurnal tide: 2. Nonmigrating tide, *J. Geophys. Res.*, doi:10.1029/2007JA012543, in press.

Yuan, T., et al. (2006), Seasonal variation of diurnal perturbations in mesopause region temperature, zonal, and meridional winds above Fort Collins, Colorado (40.6°N, 105°W), *J. Geophys. Res.*, *111*, D06103, doi:10.1029/2004JD005486.

Yudin, V. A., M. A. Geller, B. V. Khattatov, D. A. Ortland, M. D. Burrage, C. McLandress, and G. G. Shepherd (1998), TMTM simulations of tides: Comparison with UARS observations, *Geophys. Res. Lett.*, *25*(2), 221–224, doi:10.1029/97GL03584.

M. E. Hagan, T. L. Killeen, H.-L. Liu, R. G. Roble, S. C. Solomon, and Q. Wu, High Altitude Observatory, National Center for Atmospheric Research, P.O. Box 3000, Boulder, CO 80307-3000, USA. (qwu@ucar.edu)

R. J. Niciejewski and W. R. Skinner, Space Physics Research Laboratory, University of Michigan, 2455 Hayward Street, Ann Arbor, MI 48109-2143, USA.

D. A. Ortland, Northwest Research Associates, P.O. Box 3027, Bellevue, WA 98009-3027, USA.

J. Xu, Key Laboratory for Space Weather, Center for Space Science and Applied Research, Chinese Academy of Sciences, P.O. Box 8701, Beijing, China 100080.